ORGANOMETALLICS
Article
pubs.acs.org/Organometallics

Aggregation-Induced Emission of Bis(imino)acenaphthene Zinc Complexes: Photophysical Tuning via Methylation of the Flanking Aryl Substituents

Daniel A. Evans,[†] Lucia Myongwon Lee,[‡] Ignacio Vargas-Baca,[‡] and Alan H. Cowley*[,†]

[†]Department of Chemistry, The University of Texas at Austin, 1 University Station A5300, Austin, Texas 78712-0165, United States
[‡]Department of Chemistry and Chemical Biology, McMaster University, Hamilton, Ontario, Canada L8S 4M1

Supporting Information

ABSTRACT: Bis(imino)acenaphthene zinc complexes with methylated aryl substituents have been examined from the standpoint of their photoluminescent properties. Although complexes **1**−**4** proved to be nonemissive in solution, complexes **1** and **2** were found to emit via an aggregation-induced emission pathway. On the other hand, complexes **3** and **4** were found to be nonemissive in the solid state. Detailed crystallographic studies of complexes **1**−**4** provided valuable insights into the structural differences between the emissive (**1** and **2**) and nonemissive complexes (**3** and **4**), particularly with respect to their molecular structures and crystal-packing environments. TD-DFT theoretical calculations were carried out and were found to support the hypothesis that the phosphorescent emissions of **1** and **2** are due to the existence of intermolecular π-stacking interactions within the crystal lattices. Finally, a series of solvatomorphs of complexes **1** and **2** were synthesized and their emissive properties were studied.

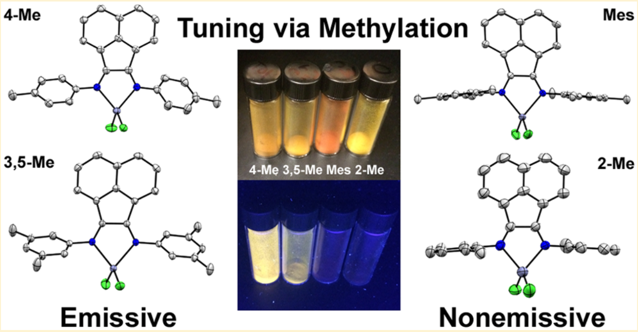

INTRODUCTION

Organic-based emissive materials continue to attract significant attention due to their applications in a variety of solid-state optoelectronic devices.[1] Unfortunately, however, the intensities of the emissions for such materials are typically reduced in the solid state in comparison with those of their solution-based counterparts.[2] Quenching of this type is generally attributed to noncovalent intramolecular interactions such as $\pi-\pi$ interactions or hydrogen bonding and is commonly referred to as "aggregation-caused quenching" (ACQ).[3] In particular, ACQ represents a serious problem for the fabrication of solid-state optoelectronic devices. As a consequence, numerous approaches have been taken in an effort to overcome this obstacle. One such approach involves the installation of sterically encumbered groups in order to inhibit aggregate formation.[4] However, despite such efforts, the ACQ effect remains a serious problem because aggregate formation is an inherent process that takes place spontaneously upon formation of a solid-state material.

In a major 2001 breakthrough, Tang et al. discovered materials that exhibited enhanced emissions in the aggregate state and referred to this type of behavior as aggregate-induced emission (AIE).[5] In contrast to the behavior of materials that display ACQ, the propeller-shaped phenyl-substituted silole materials synthesized by Tang et al. were found to inhibit $\pi-\pi$ interactions upon aggregation. Furthermore, the phenyl rotors, which provide a nonradiative pathway in solution due to dynamic intramolecular rotations, become restricted in the solid state. As a consequence, the foregoing restrictions of intramolecular rotations (RIR) provide a radiative decay pathway.[6] Currently, AIE materials represent an exciting new approach to solid-state emissive materials.[7]

An excellent example of the value of AIE is evident in the elegant work of Hariharan et al.[8] In this study, the pyrene lumiphore was acylated in a stepwise fashion, thereby changing the crystal packing environments in a controlled manner. In turn, this stepwise acylation resulted in a steady decrease of the interplanar angle between the adjacent pyrene units, thereby causing an increase in $\pi-\pi$ orbital overlap. In turn, the foregoing structural modifications resulted in an alteration in the crystal packing, thus effecting an overall change in the photophysical properties of each acylated pyrene molecule.

Bis(imino)acenaphthene (BIAN) ligands are well-known bidentate nitrogen donors that have many important applications, most notably as ligand frameworks for the support of olefin polymerization catalysts.[9] Moreover, BIAN ligands have been shown to possess several features that are desirable for photophysical applications such as a π-conjugated naphthalene backbone, structural rigidity, and the presence of tunable flanking aryl substituents. Nevertheless, despite the

Special Issue: Mike Lappert Memorial Issue

Received: November 25, 2014

© XXXX American Chemical Society

DOI: 10.1021/om501191c

foregoing advantages, BIAN ligands have seldom been used in a photophysical context.[10] We have previously used the BIAN ligand extensively, and therefore interest was generated in the use of this ligand for potential photoluminescent applications.[11] Accordingly, the work reported herein is focused on the systematic tuning of a series of methylated aryl-substituted BIAN Zn(II) complexes that exhibit solid-state photoluminescence via aggregation-induced emissions.

RESULTS AND DISCUSSION

The syntheses of the pertinent Ar-BIAN zinc complexes were carried out by means of the facile condensation reactions of acenaphthenequinone with two equivalents of the appropriate methyl-substituted anilines in the presence of anhydrous zinc chloride.[12] Each of the resulting mixtures was subsequently refluxed in acetic acid for 1 h, thus forming the corresponding BIAN zinc complex as a precipitate. Decomplexation can be achieved readily by refluxing each BIAN zinc complex in an aqueous solution of potassium oxalate for an appropriate period of time.

As mentioned previously, the free BIAN ligand platform is used extensively. However, the BIAN zinc chloride complex that is generated during the synthesis of the BIAN ligand is typically viewed as merely a synthetic stepping stone that is necessary for the preparation of the more widely used free BIAN ligand. It therefore came as a pleasant surprise to discover that the typically neglected BIAN zinc chloride intermediate complexes exhibited some very interesting photoluminescent properties.

Scheme 1. Syntheses of Ar-BIAN Zinc Complexes 1−4

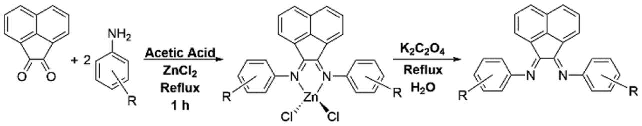

R = 4-Me (1), 3,5-Me (2), 2,4,6-Me (3), 2-Me (4)

The serendipitous discovery of the foregoing photoluminescent complexes prompted our investigation into an enhanced understanding of the origin of such emissions. The BIAN ligand platform is noted for facile tunability via modification of the stereoelectronic properties of the flanking aryl substituents. However, the present work is confined to the photoluminescent properties of the BIAN complexes that feature methylated aryl substituents, namely, *p*-methylphenyl (4-Me), 3,5-dimethylphenyl (3,5-Me), 2,4,6-trimethylphenyl (Mes), and *o*-methylphenyl (2-Me) substituents. The foregoing aryl substituents were selected in order to probe the photoluminescent properties of each individual BIAN zinc complex while holding the electronic effects relatively constant. The four methylated Ar-BIAN zinc chloride complexes in question, namely, 4-Me (**1**), 3,5-Me (**2**), Mes (**3**), and 2-Me(**4**), were synthesized according to the pertinent literature procedures.[12,13] Although these complexes had been synthesized previously, their emissive properties and solid-state structures had yet to be investigated.

Initially, the photophysical properties of complexes **1**−**4** were probed by means of UV/vis absorption spectroscopy that was carried out in DCM solution at room temperature. As exhibited in Figure 1, each of the spectra displays similar features. In accord with previously published studies, the high-energy bands (>350 nm) have been assigned as $\pi-\pi^*$ transitions that emanate from both the flanking aryl groups and the acenaphthene backbone.[14] As described by Zysman-Colman et al., on the basis of DFT calculations, the lower energy bands were tentatively attributed to intraligand charge transfer (^{1}ILCT) between the flanking arylimine fragments and the acenaphthene backbone.[15] A summary of the pertinent solution-based UV/vis spectroscopic data is presented in Table 1.

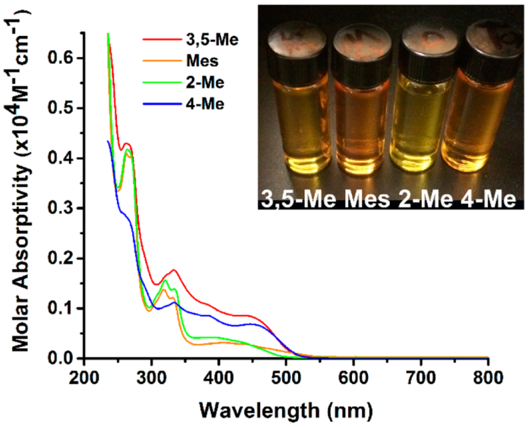

Figure 1. UV/vis absorption spectra of complexes **1**−**4** in DCM solution.

Table 1. Solution-Based UV/Vis Spectroscopic Data for Complexes 1−4

complex	λ_{max} (nm) ($\varepsilon \times 10^4$ M^{-1} cm^{-1})
1	447 (0.68), 334 (1.12), 259 (2.89)
2	437 (0.86), 333 (1.76), 262 (4.30)
3	408 (0.32), 332 (1.21), 318 (1.38), 263, (4.09)
4	387 (0.42), 334 (1.39), 321 (1.56), 264 (4.17)

Subsequent investigations were focused on the solid-state diffuse reflectance spectra of complexes **1**−**4**. As displayed in Figure 2, the reflectance spectra for all four BIAN zinc complexes are characterized by the presence of an intense absorption band between 450 and 550 nm. In the case of **3**, the absorption band features a prominent shoulder at 520 nm. Interestingly, despite the similarities in their absorption spectra, the 4-Me and 3,5-Me BIAN zinc chloride complexes were found to exhibit yellow emissions centered at 570 and 575 nm, respectively. On the other hand, the Mes and 2-Me BIAN zinc complexes turned out to be nonemissive in the solid state. The emissions from **1** and **2** were identified as being phosphorescent on the basis of their microsecond lifetimes (τ) both at room temperature and also at liquid nitrogen temperature, as displayed in Table 2. Complexes **1** and **2** exhibited low absolute quantum yields (Φ) (see Table 2). Furthermore, all four BIAN zinc complexes were found to be nonemissive in solution.

In order to gain further insight into the characteristics of the emissions from complexes **1** and **2**, it became necessary to perform a series of AIE experiments. For this purpose, a dichloromethane (DCM) stock solution of **1** was used for the preparation of the various volumetric fractions of DCM/hexanes, the overall objective being to confirm the existence of an AIE mechanism for the emission of complex **1**. As evident from Figure 3, complex **1** is nonemissive in translucent DCM/hexanes mixtures up to a volumetric ratio of 50% DCM/50%

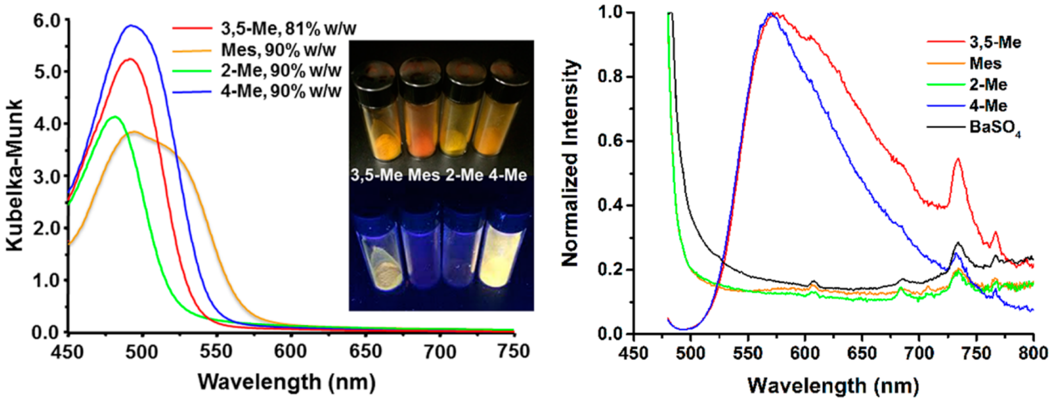

Figure 2. Absorption (top) and emission (bottom) spectra of complexes **1**−**4** in the solid state along with optical images of these complexes under both ambient light and UV irradiation.

Table 2. Solid-State Fluorescence Data for 1 and 2

complex	λ_{em} (nm)	λ_{ex} (nm)	τ (μs)	Φ (%) (absolute)
1	570	470	2.60 ± 0.79 (298 K) 3.99 ± 1.26 (77 K)	1.69 ± 0.06
2	575	470	6.21 ± 0.70 (298 K) 6.88 ± 1.17 (77 K)	1.01 ± 0.13

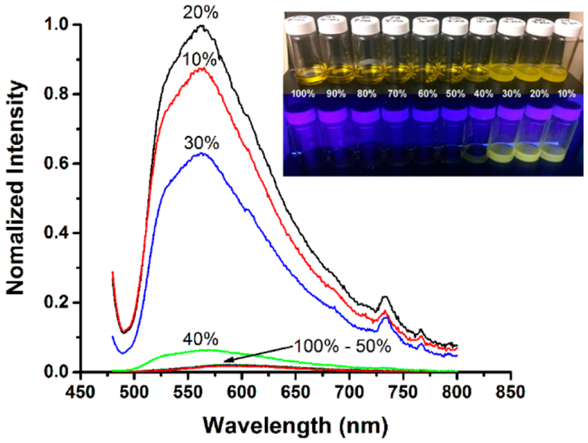

Figure 3. AIE emission spectra and photographs of the corresponding volumetric fractions (~10^{-4} M) of the DCM/hexanes mixtures of complex **1** under ambient light and UV irradiation.

hexanes. However, upon formation of a 40% DCM/60% hexanes mixture, complex **1** began to precipitate and only faint emission was detectable. Furthermore, this emission was found to be intensified in the 30−10% DCM fractions as displayed in Figure 3. A similar behavior was evident for the AIE experiment that was carried out on complex **2** using a series of THF/hexanes volumetric mixtures. Additional details regarding the latter experiment can be found in the Supporting Information.

The question that arose regarding the origins of the solid-state emissions of **1** and **2** (as opposed to their nonemissive behavior in solution) was addressed by means of a series of AIE experiments. Unfortunately, however, the acquired information failed to provide a satisfactory explanation for the nonemissive behavior of complexes **3** and **4** either in solution or in the solid state. In order to address this issue, the structure−property relationships of all four complexes were investigated by means of single-crystal X-ray diffraction studies. Surprisingly, in the cases of complexes **1**−**3**, a crop of crystals suitable for single-crystal X-ray diffraction studies was obtained directly from the precipitate that had formed in the refluxing acetic acid solution. In contrast, satisfactory single crystals of complex **4** could be grown by slow evaporation of a DCM solution.

Initial inspection of the crystal structures of complexes **1**−**4** revealed an obvious structural dichotomy between the emissive complexes **1** and **2** and those of the nonemissive complexes **3** and **4**, as evident from Figure 4. Complexes **1** and **2** were found to exhibit average acenaphthene−aryl interplanar torsion angles of 58.76° and 69.77°, respectively. In contrast, complexes **3** and **4** feature average acenaphthene−aryl interplanar torsion angles of 80.47° and 81.79°, respectively. The foregoing differences in the molecular structures could be attributed to the presence of methyl groups on the 2- and/or 6-positions of the flanking aryl substituents of complexes **3** and **4**, which are of course absent in the cases of **1** and **2**. In turn, the presence of the latter methyl substituents restricts the rotation of the flanking aryl rings. In contrast to the behavior of complexes **1** and **2**, the restricted intramolecular rotations of **3** and **4** orient the flanking aryl substituents and the naphthalene backbone in a virtually orthogonal manner.

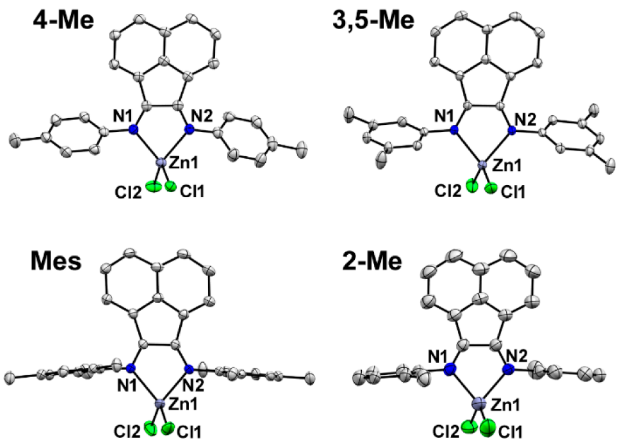

Figure 4. POV-Ray diagrams for complexes **1**−**4** with thermal ellipsoids displayed at 50% probability. All hydrogen atoms have been removed for clarity. Note, however, that complex **2** crystallized with two molecules in the asymmetric unit. One of these molecules has been removed for clarity.

As a consequence of the presence of different methylated aryl substituents, the crystal packing environments for complexes

1−**4** fall into two distinct catagories. As displayed in Figure 5, complexes **1** and **2** are closely packed and feature parallel displaced, head-to-tail $\pi-\pi$ stacking. Moreover, complex **1** comprises an extended array of $\pi-\pi$ stacking columns that are arranged in an overall staircase motif. Furthermore, the latter staircase formation packs in a head-to-tail fashion as a result of the $\pi-\pi$ stacking of two naphthalene units in conjunction with a close contact interaction between a chlorine atom and both carbons of the N−C−C−N fragment. Similarly, complex **2** also packs in a parallel displaced $\pi-\pi$ stacking motif along with two other BIAN complexes that flank this arrangement in an orthogonal manner. The foregoing face-to-face $\pi-\pi$ stacking of the naphthalene moieties is known to be conducive to excimer formation.[16]

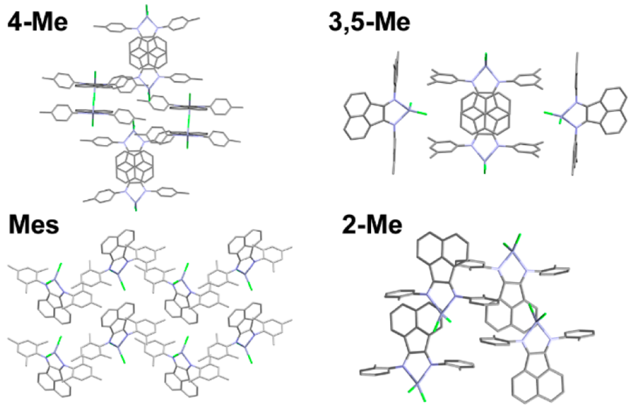

Figure 5. Crystal packing diagrams for complexes **1**−**4**.

Interestingly, complexes **3** and **4** do not involve $\pi-\pi$ stacking and consequently pack in a less dense, herringbone fashion. As mentioned earlier, the *ortho*-substituted aryl groups orient the molecular structure in an orthogonal fashion. In turn, this orthogonal orientation apparently inhibits $\pi-\pi$ stacking due to the existence of steric repulsion. By contrast, steric repulsion of this type is absent in complexes **1** and **2**; hence these complexes possess more acute interplanar aryl-acenaphthene torsion angles. Overall, the differences in these torsion angles result in the formation of a less dense crystal packing environment for both **3** and **4** in comparison with those for **1** and **2**. Collectively, the herringbone packing environments of **3** and **4** do not feature $\pi-\pi$ stacking and could therefore inhibit excimer formation, thus resulting in nonemissive behavior.

In an effort to further elucidate the nature of the emissions from complexes **1** and **2**, it became desirable to carry out some pertinent theoretical calculations. By means of TD-DFT calculations (ADF, TZP, SAOP), it was possible to confirm the viability of intermolecular electron excitations within the π-stacked dimer of **1**. Furthermore, it was determined that the lowest triplet states lie below those of the first singlet states. The triplet to singlet transitions that would radiatively relax can be visualized by plotting the transition densities (Figure 6) according to the expression $\rho_{ge}(r) = \psi_g{}^*(r)\ \psi_e(r)$.

As a result of the TD-DFT calculations, it can be surmised that small changes in the crystal packing environments could perturb the intramolecular electron excitations and thus change the emissive properties of complexes **1** and **2**. With this in mind, polymorphism was investigated as a means of tuning the emissions of complexes **1** and **2**.

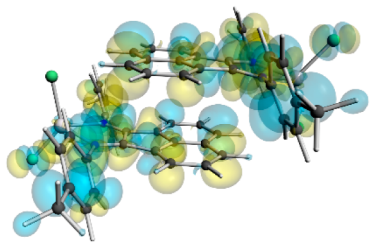

Figure 6. Transition density for the first triplet → singlet transition.

Polymorphism represents an effective way of tuning the photophysical properties of solid-state materials by engineering the crystal packing environments. Not surprisingly, this approach has been used extensively as a successful pathway for tunability.[17] Moreover, in related work, solvatomorphism has been employed for effecting subtle changes in the solid-state luminescent properties by the incorporation of different solvent molecules into the crystal lattice.[18]

Surprisingly, four solvatomorph structures could be grown for each complex merely by changing the solvent that was used for recrystallization. As displayed in Figure 7, each solvatomorph of **1** and **2** features a similar packing arrangement of parallel displaced $\pi-\pi$ stacking interactions. In this respect, each solvatomorph of complex **1** is reminiscent of the nonsolvated lattice of **1** in the sense that each lattice features infinite $\pi-\pi$ stacking columns that are arranged in a staircase formation. Interestingly, each solvatomorph of complex **2** features an alternate parallel slipped $\pi-\pi$ stacking staircase formation. The solvatomorphs of complex **2** stack in this fashion as a consequence of both the $\pi-\pi$ contacts between naphthalene units and the Cl−H contacts of the flanking aryl groups. The calculated crystallographic details involving the distances and angles of the slipped $\pi-\pi$-stacked naphthalene rings are summarized in Table 3.

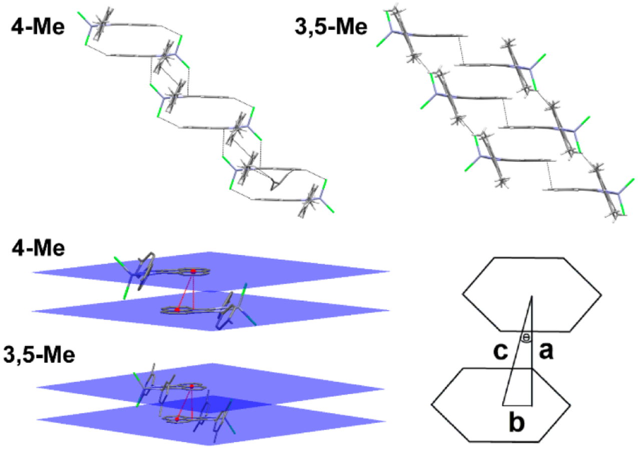

Figure 7. Stacking interactions of solvatomorphs for complexes **1** and **2** (top). Slipped stacked $\pi-\pi$ interactions (bottom): a = interplanar distance, b = slip distance of naphthalene centroids, c = distance between naphthalene centroids, θ = slip angle between naphthalene centroids.

As displayed in Table 3, each solvatomorph features a slightly different crystal packing environment and consequently exhibits different photophysical properties. Figure 8 exhibits the various crystalline samples that were examined by both fluorescence spectroscopy and fluorescent microscopy. A summary of the

Table 3. Calculated Crystallographic Details of Solvatomorph $\pi-\pi$ Interactions

solvatomorph	*a*	*b*	*c*	*θ*
1	3.504 Å	1.439 Å	3.788 Å	22.33°
1-$CHCl_3$	3.418 Å	1.266 Å	3.645 Å	20.33°
1-THF	3.421 Å	1.415 Å	3.702 Å	22.47°
1-DCM	3.569 Å	1.604 Å	3.787 Å	19.54°
1-MeCN	3.549 Å	1.400 Å	3.815 Å	21.52°
2	3.725 Å	1.763 Å	4.121 Å	25.32°
2-$CHCl_3$	3.431 Å	1.300 Å	3.668 Å	20.71°
2-THF	3.404 Å	1.246 Å	3.625 Å	20.10°
2-DCM	3.400 Å	1.328 Å	3.650 Å	21.33°
2-MeCN	3.450 Å	1.228 Å	3.662 Å	19.59°

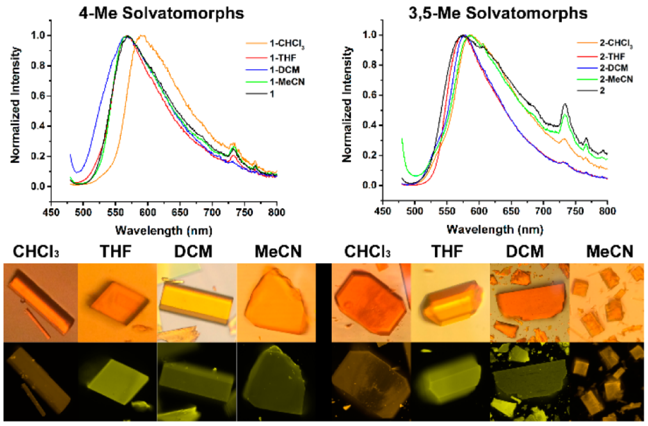

Figure 8. Emission spectra, optical, and fluorescent images for the solvatomorphs of complexes **1** and **2**.

photophysical data for each solvatomorph can be found in Table 4.

Table 4. Solid-State Fluorescence Data for Solvatomorphs of Complexes 1 and 2

complex	λ_{em} (nm)	λ_{ex} (nm)	τ (μs)	Φ (%) (relative)[a]
1-$CHCl_3$	590	470	4.59 ± 1.12	3.78 ± 0.13
1-THF	567	470	2.97 ± 0.96	1.52 ± 0.14
1-DCM	569	470	6.23 ± 1.17	0.35 ± 0.01
1-MeCN	569	470	2.86 ± 0.57	0.63 ± 0.02
2-$CHCl_3$	587	470	4.94 ± 0.09	1.03 ± 0.13
2-THF	576	470	4.51 ± 0.75	2.59 ± 0.32
2-DCM	578	470	4.54 ± 1.02	2.42 ± 0.30
2-MeCN	585	470	6.41 ± 1.33	0.84 ± 0.10

[a] The relative quantum yield values were calculated based on the ratio of the emission intensities. The intensity of the emission peak for each solvatomorph was integrated and compared with that of the nonsolvated complex, for which the absolute quantum yield had been measured directly.

The most significant change in photophysical properties was observed in the case of the $CHCl_3$ solvatomorph of complex **1**. This particular solvatomorph was found to be red-shifted by approximately 20 nm in comparison with those of the other three solvatomorphs of complex **1**. This outcome is presumably due to the increased $\pi-\pi$ orbital overlap of this solvatomorph in comparison with the other solvatomorphs of complex **1**. Furthermore, the solvatomorphs of complex **2** exhibit a more subtle shift in lambda max with respect to the solvatomorphs of complex **1**. Specifically, the solvatomorphs of complex **2** that contain $CHCl_3$ and MeCN were found to be red-shifted by approximately 10 nm in comparison with those of the THF and DCM solvatomorphs (Table 4).

In summary, four methylated Ar-BIAN complexes have been investigated from the standpoint of their photophysical properties. Complexes **1** and **2** were found to be emissive via AIE pathways. In contrast, complexes **3** and **4** proved to be nonemissive in both the solid state and in solution. Analyses of the crystal packing diagrams for complexes **1**−**4** provided valuable insights into the possible reasons for both the emissive behavior of complexes **1** and **2** and also for the nonemissive behavior of complexes **3** and **4**. The hypothesis for the origin of the emissions of complexes **1** and **2** was supported on the basis of TD-DFT calculations. Furthermore, a solvatomorph study was performed in order to investigate the effect that subtle changes in crystal packing environments would have on the emissive properties of each complex. Future effort will be focused on tuning the stereoelectronic properties of the BIAN ligand class in order to modify and control the photophysical properties of the BIAN zinc complexes.

■ EXPERIMENTAL SECTION

General Procedures. All reactions were performed in the ambient atmosphere with glassware that had been oven-dried and flushed with argon gas prior to use. The *p*-methylphenyl (**1**),[12] 3,5-dimethylphenyl (**2**),[12] 2,4,6-trimethylphenyl (**3**),[12] and *o*-methylphenyl (**4**)[13] BIAN zinc chloride complexes were synthesized according to the pertinent literature procedures.

Physical Measurements. All of the NMR spectra were recorded at 298 K on either a Varian DirectDrive instrument (^1H NMR, 599.75 MHz; ^{13}C NMR, 150.82 MHz) or a Varian INOVA instrument (^1H NMR, 499.87 MHz; ^{13}C NMR, 125.71 MHz), using residual solvent as the internal reference. The deuterated chloroform solvent was procured from Cambridge Isotopes Laboratories, Inc., and stored over 4 Å molecular sieves prior to use. The high-resolution chemical ionization mass spectral data (HRMS-CI) were collected on a Micromass Autospec Ultima mass spectrometer. The melting points of **1**−**4** were determined using a Mel-Temp apparatus. Samples of complexes **1**−**4** were sent to Midwest Microlab, LLC, for C, H, and N elemental analyses.

Fluorescence Spectroscopy. All solid-state fluorescence spectroscopy experiments were performed on a Photon Technology International QM 4 spectrophotometer equipped with a 6 in. diameter K Sphere-B integrating sphere. The crystalline powders of **1**−**4** were loaded into quartz EPR tubes for measurement purposes, and their chemical identities were confirmed by powder X-ray crystallography. All solvatomorph samples were loaded into quartz EPR tubes and subsequently covered with mineral oil to maintain crystallinity. The absolute quantum yield measurements were made by using a 6 in. diameter K Sphere-B integrating sphere. The absolute quantum yield values were calculated by dividing the integrated area under each emission curve by the respective excitation peak of each sample. $[(\mathrm{Area}_{\text{sample emission}}/(\mathrm{Area}_{\text{BaSO4 blank excitation}} - \mathrm{Area}_{\text{sample excitation}})]$. The relative quantum yield values were calculated based on the ratio of the emission intensities. The intensity of the emission peak for each solvatomorph was integrated and compared with that of the nonsolvated complex, for which the absolute quantum yield had been measured directly. All graphs were constructed using the OriginPro 9.1 Student Version 64bit program.

Single-Crystal X-ray Crystallography. In the cases of compounds **1**−**3**, suitable single crystals could be obtained directly from each reaction mixture. Suitable crystals of complex **4** were grown via slow evaporation of a dichloromethane solution of this complex. Each solvatomorph crystal was grown from the appropriate solvent. In each case, the single crystals were removed from their respective vials, covered with mineral oil, and mounted separately on nylon thread loops. The X-ray diffraction data (powder and single crystal) were collected on an Agilent Technologies SuperNova Dual Source diffractometer using a μ-focus Cu Kα radiation source (λ = 1.5418 Å) equipped with collimating mirror monochromators. Crystals **1** and **2** were collected at 100 K, and crystals **3** and **4** were collected at 147 K. All solvatomorphs were collected at 133 K. Crystallographic details for all structures can be found in the Supporting Information. Data collection, unit cell refinement, and data reduction were performed using the Agilent Technologies CrysAlisPro V 1.171.37.31 program.[19] The structure of each complex was solved by direct methods using the SIR97[20] program and refined by full-matrix least-squares on F^2 with anisotropic displacement parameters for all non-H atoms using SHELXL-2013.[21] The structural analyses were performed using the PLATON98[22] and WinGX[23] programs, and all non-hydrogen atoms were refined anisotropically. The hydrogen atoms were placed in fixed, calculated positions with isotropic displacement parameters set to 1.2 × U_{eq} with respect to the attached atom (1.5 × U_{eq} for methyl hydrogens). All powder XRD graphs were constructed using the OriginPro 9.1 Student Version 64 bit program. The POV-Ray images were created using the Mercury version 3.3 program. The crystallographic details concerning the solvatomorph $\pi-\pi$ interactions were calculated using the Mercury version 3.3 program.

Diffuse-Reflectance and UV/Vis Absorption Spectroscopy. All diffuse-reflectance measurements were performed with an illuminated (tungsten-halogen light source) integrating sphere (Ocean Optics ISP-REF) attached to a photodiode array spectrophotometer (Ocean Optics SD 2000), and all data are reported relative to a $BaSO_4$ standard. Each measurement was integrated over 3 ms and corrected for stray light and dark current. The raw data were used to calculate the reflectance (R) using Grams/AI (version 8.0). The Kubelka−Munk function ($[1 - R]^2/2R$) was evaluated in Excel, and the resulting spectra were smoothed by calculating the weighted averages of the values at neighboring points using the Cauchy density function as implemented within SigmaPlot (version 9). The final illustration was composed in PowerPoint. All UV/vis absorption experiments were performed using a Varian Vary 6000i UV−vis−NIR spectrophotometer. All UV/vis graphs were constructed using the OriginPro 9.1 Student Version 64bit program.

DFT Calculations. All DFT calculations were performed using the ADF DFT package (version 2013).[24,25] A model of the π-stacked dimer of complex **1** was built from the crystallographic coordinates, and the positions of all non-carbon atoms were optimized using the exchange−correlation functional of Perdew, Burke, and Ernzerhof[26] and corrected for dispersion[27] with a triple-ζ all-electron basis set with two polarization functions and applying the zeroth-order regular approximation (ZORA)[28−32] formalism with specially adapted basis sets. In the interest of expediency, the lowest 80 singlet−singlet and lowest 80 singlet−triplet electronic excitations[33,34] were calculated using time-dependent density functional theory (TD-DFT) under the statistical average of different model potentials for occupied KS orbitals (SAOP).[35−37]

Fluorescent Microscopy. The fluorescent microscopy was performed on a Zeiss Axiovert200 M epifluorescent microscope. The crystalline solvatomorph samples were excited using an FITC filter cube. The fluorescent microscopy images were created using the program Axiovision 4.6.

Syntheses of 1−4. *4-Methylphenyl-BIAN Zinc Chloride (**1**).* A mixture of acenaphthenequinone (1.00 g, 5.49 mmol) and anhydrous zinc chloride (2.02 g, 14.82 mmol) was suspended in 10 mL of glacial acetic acid, thereby generating a yellow suspension. The latter yellow suspension was heated to 60 °C, and *p*-toluidine (1.42 mL, 12.63 mmol) was added, following which the resulting solution was refluxed for 1 h. The precipitate that had formed during the latter reaction was filtered off and washed sequentially with water and diethyl ether. The resulting crystalline, yellow-orange powder was collected and used without further purification for a single-crystal X-ray diffraction study (2.18 g, 80%).

HRMS (CI, CH_4): calcd for $[M - Cl]^+$ $[C_{26}H_{20}N_2ZnCl]^+$ m/z 459.0606; found 459.0605. ^1H NMR ($CDCl_3$): δ 2.464 (s, 6H, CH_3), 7.363 (d, 4H, Ar−H, J = 8.0 Hz), 7.511 (d, 4H, Ar−H, J = 8.0 Hz), 7.598 (t, 2H, Ar−H, J = 7.7 Hz), 7.650 (d, 2H, Ar−H, J = 7.2 Hz), 8.132 (d, 2H, Ar−H, J = 8.1 Hz). ^{13}C NMR ($CDCl_3$): δ 21.35, 121.69, 125.33, 125.96, 128.56, 130.66, 131.14, 132.26, 139.20, 141.07, 144.88, 161.85. MP: 344 °C. Anal. Calcd for $C_{26}H_{20}N_2ZnCl_2$: C, 62.87; H, 4.06; N, 5.64. Found: C, 62.84; H, 3.99; N, 5.54.

*3,5-Dimethylphenyl-BIAN Zinc Chloride (**2**).* A mixture of acenaphthenequinone (1.00 g, 5.49 mmol) and anhydrous zinc chloride (2.02 g, 14.82 mmol) was suspended in 10 mL of glacial acetic acid, thereby generating a yellow suspension. The latter yellow suspension was heated to 60 °C, and 3,5-dimethylaniline (1.49 mL, 12.63 mmol) was added, following which the resulting solution was refluxed for 1 h. The precipitate that had formed during the latter reaction was filtered off and washed sequentially with water and diethyl ether. The resulting crystalline yellow powder was collected and used without further purification for a single-crystal X-ray diffraction study (1.84 g, 64%).

HRMS (CI, CH_4): calcd for $[M - Cl]^+$ $[C_{28}H_{24}N_2ZnCl]^+$ m/z 487.0919; found 487.0913. ^1H NMR ($CDCl_3$): δ 2.404 (s, 12H, CH_3), 7.102 (s, 2H, Ar−CH_3), 7.179 (s, 4H, Ar−CH_3), 7.536 (d, 2H, Ar−H, J = 6.5 Hz), 7.607 (d, 2H, Ar−H, J = 7.8 Hz), 8.147 (d, 2H, Ar−H, J = 8.2 Hz). ^{13}C NMR ($CDCl_3$): δ 21.38, 118.82, 125.27, 126.05, 128.60, 130.37, 131.08, 132.19, 140.03, 162.12. MP: 321 °C. Anal. Calcd for $C_{28}H_{24}N_2ZnCl_2$: C, 64.08; H, 4.61; N, 5.34. Found: C, 64.06; H, 4.62; N, 5.28.

*2,4,6-Trimethylphenyl-BIAN Zinc Chloride (**3**).* A mixture of acenaphthenequinone (1.00 g, 5.49 mmol) and anhydrous zinc chloride (2.02 g, 14.82 mmol) was suspended in 10 mL of glacial acetic acid, thereby generating a yellow suspension. The latter yellow suspension was heated to 60 °C, and 2,4,6-trimethylphenylaniline (1.64 mL, 12.63 mmol) was added, following which the resulting solution was refluxed for 1 h. The precipitate that had formed during the latter reaction was filtered off and washed sequentially with water and diethyl ether. The resulting crystalline red powder was collected and used without further purification for a single-crystal X-ray diffraction study (2.69 g, 89%).

HRMS (CI, CH_4): calcd for $[M - Cl]^+$ $[C_{30}H_{28}N_2ZnCl]^+$ m/z 515.1232; found 515.1237. ^1H NMR ($CDCl_3$): δ 2.313 (s, 12H, CH_3), 2.405 (s, 6H, CH_3), 6.936 (d, 2H, Ar−H, J = 7.4 Hz), 7.063 (s, 4H, Ar−H), 7.602 (dd, 2H, Ar−H, J = 7.8 Hz, 1.0 Hz), 8.153 (d, 2H, Ar−H, J = 8.0 Hz). ^{13}C NMR ($CDCl_3$): δ 18.36, 21.02, 125.57, 125.87, 128.36, 129.33, 129.97, 130.97, 132.36, 137.24, 140.28, 144.43, 164.20. MP: 384 °C. Anal. Calcd for $C_{30}H_{28}N_2ZnCl_2$: C, 65.18; H, 5.11; N, 5.07. Found: C, 65.18; H, 5.13; N, 5.02.

*2-Methylphenyl-BIAN Zinc Chloride (**4**).* A mixture of acenaphthenequinone (1.00 g, 5.49 mmol) and anhydrous zinc chloride (2.02 g, 14.82 mmol) was suspended in 10 mL of glacial acetic acid, thereby generating a yellow suspension. The latter yellow suspension was heated to 60 °C, and *o*-toluidine (1.35 mL, 12.63 mmol) was added, following which the resulting solution was refluxed for 1 h. The precipitate that had formed during the latter reaction was filtered off and washed sequentially with water and diethyl ether. The resulting crystalline yellow powder was collected and subsequently recrystallized from dichloromethane solution. The resulting crop of crystals proved to be suitable for a single-crystal X-ray diffraction study (1.47 g, 53%).

HRMS (CI, CH_4): calcd for $[M - Cl]^+$ $[C_{26}H_{20}N_2ZnCl]^+$ m/z 459.0606; found 459.0610. ^1H NMR ($CDCl_3$): δ 2.355 (s, 6H, CH_3), 6.974 (apparent dd, 2H, Ar−H, J = 7.2 Hz), 7.391 (m, 8H, Ar−H), 7.573 (dd, 2H, Ar−H, J = 8.3 Hz, J = 1.0 Hz), 8.133 (d, 2H, Ar−H, J = 8.1 Hz); ($CDCl_3$): δ 18.04, 18.28, 120.63, 120.93, 125.50, 125.51, 126.10, 127.74, 127.83, 128.08, 128.11, 128.76, 128.94, 129.12, 131.00, 132.02, 131.66, 131.68, 132.40, 132.42, 143.37, 143.41, 144.85, 144.89, 163.51, 163.52. MP: 359 °C. Anal. Calcd for $C_{26}H_{20}N_2ZnCl_2$: C, 62.87; H, 4.06; N, 5.64. Found: C, 62.80; H, 4.13; N, 5.59.

■ ASSOCIATED CONTENT

Ⓢ Supporting Information

Fluorescence spectroscopy and crystallographic data are provided in the Supporting Information. This material is available free of charge via the Internet at http://pubs.acs.org.

AUTHOR INFORMATION

Corresponding Author

*E-mail: acowley@cm.utexas.edu.

Notes

The authors declare no competing financial interest.

ACKNOWLEDGMENTS

The authors are grateful for the generous financial support provided by the Robert A. Welch Foundation (Grant F-0003) (AHC) and the Natural Sciences and Engineering Research Council of Canada (IVB Discovery Grant, LML Doctoral Postgraduate Scholarship). This work was made possible by the facilities of the Shared Hierarchical Academic Research Computing Network (SHARCNET: www.sharcnet.ca) and Compute/Calcul Canada.

DEDICATION

Dedicated to the memory of Professor Michael F. Lappert, an outstanding scientist and a true gentleman.

REFERENCES

(1) (a) Kamtekar, K. T.; Monkman, A. P.; Bryce, M. R. *Adv. Mater.* **2010**, *22*, 572−582. (b) Xu, H.; Chen, R.; Sun, Q.; Lai, W.; Su, Q.; Huang, W.; Lui, X. *Chem. Soc. Rev.* **2014**, *43*, 2259−3302.

(2) Figueira-Duarte, T. M.; Müllen, K. *Chem. Rev.* **2011**, *111*, 7260−7314.

(3) Birks, J. B. *Photophyiscs of Aromatic Molecules*; Wiley: London, 1970.

(4) Wang, J.; Zhao, Y.; Dou, C.; Sun, H.; Xu, P.; Ye, K.; Zhang, J.; Jiang, S.; Li, F.; Wang, Y. *J. Phys. Chem. B* **2007**, *111*, 5082−5089.

(5) (a) Luo, J.; Xie, Z.; Lam, J. W. Y.; Cheng, L.; Chen, H.; Qiu, C.; Kwok, H. S.; Zhan, X.; Liu, Y.; Zhu, D.; Tang, B. Z. *Chem. Commun.* **2001**, 1740−1741. (b) Hong, Y.; Lam, J. W. Y.; Tang, B. Z. *Chem. Soc. Rev.* **2011**, *40*, 5361−5388.

(6) Hong, Y.; Lam, J. W. Y.; Tang, B. Z. *Chem. Commun.* **2009**, 4332−4353.

(7) Mei, J.; Hong, Y.; Lam, J. W. Y.; Qin, A.; Tang, Y.; Tang, B. Z. *Adv. Mater.* **2014**, *26*, 5429−5479.

(8) Rajagopal, S. K.; Philip, A. M.; Nagarajan, K.; Hariharan, M. *Chem. Commun.* **2014**, *50*, 8644−8647.

(9) Hill, N. J.; Vargas-Baca, I.; Cowley, A. H. *Dalton Trans.* **2009**, 240−253.

(10) (a) Singh, S. K.; Dubey, S. K.; Pandey, R.; Mishra, L.; Zou, R.-Q.; Xu, Q.; Pandey, D. S. *Polyhedron* **2008**, *27*, 2877−2882. (b) Adams, C. J.; Fey, N.; Harrison, Z. A.; Sazanovich, I. V.; Towrie, M.; Weinstein, J. A. *Inorg. Chem.* **2008**, *47*, 8242−8257. (c) Kern, T.; Monkowius, U.; Zabel, M.; Knör, G. *Inorg. Chim. Acta* **2011**, *374*, 632−636. (d) Adams, C. J.; Fey, N.; Weinstein, J. A. *Inorg. Chem.* **2006**, *45*, 6105−6107.

(11) (a) Crawford, K. A.; Cowley, A. H.; Humphrey, S. M. *Catal. Sci. Technol.* **2014**, *4*, 1456−1464. (b) Evans, D. A.; Vargas-Baca, I.; Cowley, A. H. *J. Am. Chem. Soc.* **2013**, *135*, 13939−13946. (c) Evans, D. A.; Cowley, A. H. *J. Am. Chem. Soc.* **2012**, *134*, 15672−15675. (d) Vasudevan, K. V.; Butorac, R. R.; Abernethy, C. D.; Cowley, A. H. *Dalton Trans.* **2010**, *39*, 7401−7408.

(12) van Asselt, R.; Elsevier, C. J.; Smeets, W. J. J.; Spek, A. L.; Benedix, R. *Recl. Trav. Chim. Pays-Bas* **1994**, *113*, 88−98.

(13) Gasperini, M.; Ragaini, F.; Cenini, S. *Organometallics* **2002**, *21*, 2950−2957.

(14) (a) Rosa, V.; Santos, C. I. M.; Welter, R.; Aullon, G.; Lodeiro, C.; Aviles, T. *Inorg. Chem.* **2010**, *49*, 8699. (b) Rosa, V.; Aviles, T.; Aullon, G.; Covelo, B.; Lodeiro, C. *Inorg. Chem.* **2008**, *47*, 7734. (c) Paulovicova, A.; El-Ayaan, U.; Shibayama, K.; Morita, T.; Fukuda, Y. *Eur. J. Inorg. Chem.* **2001**, 2641.

(15) Hasan, K.; Zysman-Colman, E. *J. Phys. Org. Chem.* **2013**, *26*, 274−279.

(16) Zhang, H.; Zhang, Z.; Ye, K.; Zhang, J.; Wang, Y. *Adv. Mater.* **2006**, *18*, 2369−2372.

(17) (a) Li, R.; Xiao, S.; Li, Y.; Lin, Q.; Zhang, R.; Zhao, J.; Yang, C.; Zou, K.; Li, D.; Yi, T. *Chem. Sci.* **2014**, *5*, 3922−3928. (b) Dong, Y.; Xu, B.; Zhang, J.; Tan, X.; Wang, L.; Chen, J.; Lv, H.; Wen, S.; Li, B.; Ye, L.; Zou, B.; Tian, W. *Angew. Chem., Int. Ed.* **2012**, *51*, 10782−10785. (c) Galer, P.; Korošec, R. C.; Vidmar, M.; Šket, B. *J. Am. Chem. Soc.* **2014**, *136*, 7383−7394. (d) Unesaki, H.; Kato, T.; Watase, S.; Matsukawa, K.; Naka, K. *Inorg. Chem.* **2014**, *53*, 8270−8277. (e) Kitamura, C.; Ohara, T.; Kawatsuki, N.; Yoneda, A.; Kobayashi, T.; Naito, H.; Komatsu, T.; Kitamura, T. *CrystEngComm* **2007**, *9*, 644−647. (f) Talarico, A. M.; Aiello, I.; Bellusci, A.; Crispini, A.; Ghedini, M.; Godbert, N.; Pugliese, T.; Szerb, E. *Dalton Trans.* **2010**, *39*, 1709−1712. (g) Field, J. S.; Ledwaba, L. P.; Munro, O. Q.; McMillin, D. R. *CrysEngComm* **2008**, *10*, 740−747. (h) Quanrtapelle Procopio, E.; Mauro, M.; Panigati, M.; Donghi, D.; Mercandelli, P.; Sironi, A.; D'Alfonso, G.; De Cola, L. *J. Am. Chem. Soc.* **2010**, *132*, 14397−14399. (i) Luo, G.-G.; Xia, J.-X.; Fang, K.; Zhao, Q.-H.; Wu, J.-H.; Dai, J.-C. *Dalton Trans.* **2013**, *42*, 16268−16271.

(18) (a) Fan, Y.; Zhao, Y.; Ye, L.; Li, B.; Yang, G.; Wang, Y. *Cryst. Growth Des.* **2009**, *9*, 1421−1430. (b) Kuwabara, J.; Ogawa, Y.; Taketoshi, A.; Kanbara, T. *J. Organomet. Chem.* **2011**, *696*, 1289−1293. (c) Benito, Q.; Le Goff, X. F.; Maron, S.; Fargues, A.; Garcia, A.; Martineau, C.; Taulelle, F.; Kahlal, S.; Gacoin, T.; Boilot, J.-P.; Perruchas, S. *J. Am. Chem. Soc.* **2014**, *136*, 11311−13320.

(19) *CrysAlisPro*, version 1.171.37.31; Agilent Technologies UK Ltd.: Oxford, UK, 2013.

(20) Altomare, A.; Burla, M. C.; Camalli, M.; Cascarano, G. L.; Giacovazzo, C.; Guagliardi, A.; Moliterni, A. G. G.; Polidori, G.; Spagna, R. *J. Appl. Crystallogr.* **1999**, *32*, 115−119.

(21) Sheldrick, G. M. *Acta Crystallogr.* **2008**, *A64*, 112−122.

(22) Spek, A. L. *J. Appl. Crystallogr.* **2003**, *36*, 7−13.

(23) Farrugia, L. J. *J. Appl. Crystallogr.* **1999**, *32*, 837−838.

(24) te Velde, G.; Bickelhaupt, F. M.; Baerends, E. J.; Fonseca Guerra, C.; van Gisbergen, S. J. A.; Snijders, J. G.; Ziegler, T. *J. Comput. Chem.* **2001**, *22*, 931−967.

(25) Fonseca Guerra, C.; Snijders, J. G.; te Velde, G.; Baerends, E. J. *Theor. Chem. Acc.* **1998**, *99*, 391−403.

(26) Perdew, J. P.; Burke, K.; Ernzerhof, M. *Phys. Rev. Lett.* **1996**, *77*, 3865−3868.

(27) Grimme, S. *J. Comput. Chem.* **2006**, *27*, 1787−1799.

(28) van Lenthe, E.; Ehlers, A.; Baerends, E. J. *J. Chem. Phys.* **1999**, *110*, 8943−8953.

(29) van Lenthe, E.; Baerends, E. J.; Snijders, J. G. *J. Chem. Phys.* **1993**, *99*, 4597−4610.

(30) van Lenthe, E.; Baerends, E. J.; Snijders, J. G. *J. Chem. Phys.* **1994**, *101*, 9783−9792.

(31) van Lenthe, E.; van Leeuwen, R.; Baerends, E. J.; Snijders, J. G. *Int. J. Quantum Chem.* **1996**, *57*, 281−293.

(32) van Lenthe, E.; Snijders, J. G.; Baerends, E. J. *J. Chem. Phys.* **1996**, *105*, 6505−6516.

(33) van Gisbergen, S. J. A.; Snijders, J. G.; Baerends, E. J. *Comput. Phys. Commun.* **1999**, *118*, 119−138.

(34) Rosa, A.; Baerends, E. J.; van Gisbergen, S. J. A.; van Lenthe, E.; Groeneveld, J. A.; Snijders, J. G. *J. Am. Chem. Soc.* **1999**, *121*, 10356−10365.

(35) Gritsenko, O. V.; Schipper, P. R. T.; Baerends, E. J. *Chem. Phys. Lett.* **1999**, *302*, 199−207.

(36) Gritsenko, O. V.; Schipper, P. R. T.; Baerends, E. J. *Int. J. Quantum Chem.* **2000**, *76*, 407−419.

(37) Schipper, P. R. T.; Gritsenko, O. V.; van Gisbergen, S. J. A.; Baerends, E. J. *J. Chem. Phys.* **2000**, *112*, 1344−1352.